An Investigation of Chiral Tag Rotational Spectroscopy for Absolute configuration determination

Taylor Collin Smart
Shrewsbury, Massachusetts

Bachelor of Science, University of Massachusetts Amherst, 2016

A Thesis presented to the Graduate Faculty of the University of Virginia for the Degree of Master of science

Department of Chemistry

University of Virginia
August, 2018

Abstract

Rotational Spectroscopy has seen many improvements since the 1970s, from increases in sensitivity, to decreases in sample consumption and time. While it has seen widespread use in diastereomer analysis, it has faced inherent challenges in enantiomer detection. For this reason, techniques are being developed that would allow for the use of rotational spectroscopy in enantiomer analysis. In this thesis, the use of a chiral tagging method was investigated for its ability to use rotational spectroscopy for determining absolute configuration. Two test cases are presented: the determination of the absolute configuration of a bicyclic monoterpene ketone enantiomer, and the identification of a sesquiterpene alcohol enantiomer. While these cases are simple compounds for test cases, they are important tests for the effectiveness of using rotational spectroscopy for absolute configuration determination.

Acknowledgements

Writing a thesis is no small task; there are many who have supported and aided me through this stressful process. The completion of this work would have been impossible without the support from those in my research group: Channing, Kevin, Marty, and Reilly, who among the stress and late nights, provided support and revisions for me and my work. Specifically, Marty, who even while across the country in California provided insight. As well as Reilly, who provided great insight into my writing and her extreme sense of detail to my talk.

In addition to my lab members, I am thankful for Dr. Brooks Pate accepting me into his lab. When I joined the lab group, I was new to spectroscopy as my undergrad focus was in biochemistry. Yet here I was, in a physical chemistry lab, but with his guidance and the exposure to the techniques used in our lab, I am proud to call myself a physical chemist; albeit still with much to learn.

Outside of those in the lab, I have to thank my friend Tianli for her kind words and her insight when it came to revising this thesis. Without her, this document would not be what it is today. Also Julie, who was with me through many painful nights when I was questioning my ability to see this through. Lastly, I must thank my parents for their support through the years, I know that they worried for me at times, but in the end, I am happy knowing that I could make them proud.

Table of Contents

Chapter 1

Introduction

I. Rotational Spectroscopy

Historically, rotational spectroscopy has been used as a high resolution gas phase technique for structure determination of small molecules.[1-3] While rotational spectroscopy has been used since the early-mid 1900's, it has seen many technical improvements over the past 50 years that have increased resolution and bandwidth while decreasing sample consumption and measurement time.[4-5] Microwave absorption spectrometers were one of the first spectrometers used for rotational spectroscopy.[5] In the late 1970's, a pulsed Fourier transform microwave spectrometer was developed, providing increased sensitivity and resolution.[6] Shortly after this improvement, the Balle-Flygare FTMW spectrometer was developed and provided another significant improvement in sensitivity and improved linewidths.[7-8] After this development, there came another advancement in 2008: the use of a chirped-pulse Fourier transform microwave spectrometer, designed by the Pate group at the University of Virginia.[9] This technique took into account newer electronics capable of performing time domain spectroscopy at the broadband level for every acquisition. This technique once again advanced sensitivity, decreased sample consumption, and decreased measurement time.

Chiral analysis does not just require enantiomeric detection. It also requires diastereomer analysis. Diastereomers are molecules that have differences at one or more of their stereocenters, whereas enantiomers have differences at all of their stereocenters. While rotational spectroscopy saw improvements throughout the past for sensitivity, time, and sample consumption, it is inherently unable to distinguish enantiomers. This inherent inability has limited the use of

rotational spectroscopy in regards to chiral analysis. The difference in all stereocenters makes enantiomers mirror images with mirror image mass distributions, preventing identification by rotational spectroscopy. [10-11] Advancements for enantiomeric analysis will be discussed in a later chapter.

Rotational spectroscopy is a gas phase technique that measures the energy differences between quantized pure rotational states of molecules.[12] By exciting the molecules with the resonant frequencies of light with these energy transitions, emission or absorption of the analytes can be observed. These transition frequencies are based on the structure of the molecule and are determined by the molecule's rotational constants.[13] These constants are derived from the inertia of the molecule along the principal axes:

$$A = \frac{\hbar^2}{2I_A} \qquad B = \frac{\hbar^2}{2I_B} \qquad C = \frac{\hbar^2}{2I_C} \tag{1}$$

where ħ is the reduced plank's constant, I_A, I_B, and I_C are the moments of inertia along the principal axes. By convention, the largest rotational constant is associated with the a principal axis and the smallest with the b principal axis.

The transition frequency intensities vary based upon the electric dipole moment component along that direction in the principal axis system. This transition requires a permanent dipole with the intensity being proportional to the square of the dipole moment matrix element for that transition.[14] In some cases, this will result in transitions not being seen in the spectrum. The intensity of the transition is also dependent on the population of the energy level, which follows a Boltzmann distribution effected by the temperature.[12] The dependence is seen in Equation 2:

$$\frac{<N_S>}{N} = \frac{e^{-\frac{\varepsilon_S}{kT}}}{z} \; for < N_r > \ll 1 \quad (2)$$

where $<N_S>$ is the average number of molecules in state S, N is the number of molecules, ε_s is the energy of state s, *k* is the Boltzmann constant, T is the temperature of the molecule and Z is the molecular partition function. As the temperature increases, the ratio of the energy levels approaches 1. As the temperature is lowered, the population is driven to lower energies. The transitions for a rigid rotor are found by Equation 3:

$$\nu = 2B(J+1) \quad (3)$$

Where ν is the frequency of the transition, J is the rotational quantum number, and B is the B rotational constant. However, molecules are not truly rigid rotors; there are other forces that act on them. Namely, there is centrifugal force that will change the shape of the molecule as it rotates. The centrifugal force makes it necessary to include distortion constants in the calculations for frequency determination. In the simple case of the linear molecule, the inclusion of distortion is shown in Equation 4:

$$\nu_{J+1\leftarrow J} = 2B_\nu(J+1) - 4D_\nu(J+1)^3 \quad (4)$$

Here *Bv* is rotational constant B taking into account vibrational dependence, and *Dv* is the centrifugal distortion constant taking into account vibrational dependence. More distortion has to be accounted for as nonlinear molecules are investigated. The inclusion of the distortion results in a more complex equation for solving the transition frequencies, including three distortion constants. These frequencies result in a line spectrum for a molecule of interest. If there is more than one species in the pulsed jet expansion, then there would be multiple spectra found as a result of multiple species present. An example spectrum is shown in Figure 1. This is a simulated

spectrum for the lowest energy conformation of (1*R*)-1,7,7-timethylbicyclo[2.2.1]heptan-2-one (R-camphor) and (*R*)-(+)-3-butyn-2-ol (R-butynol) complex.

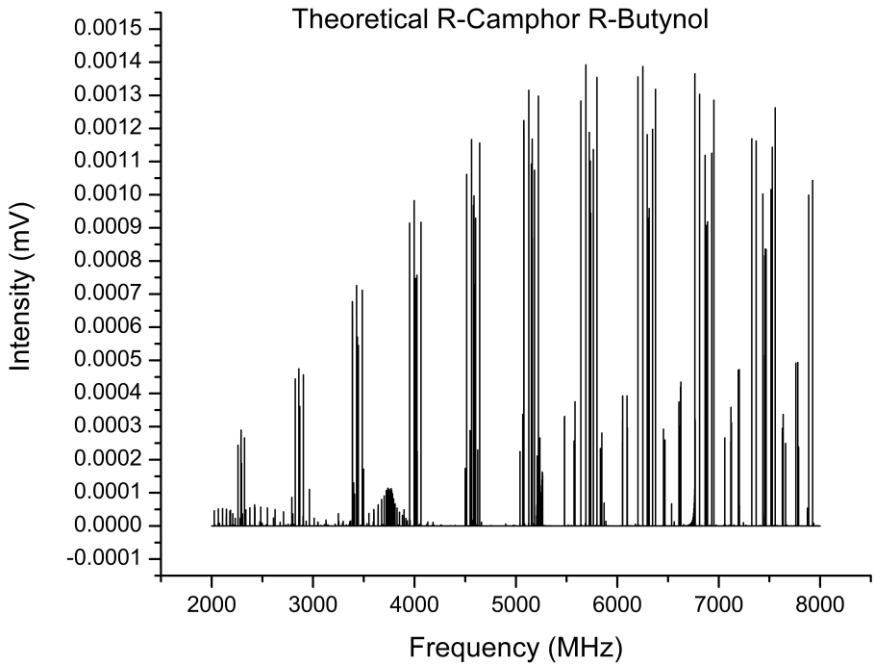

Figure 1: Simulated spectrum of the lowest energy R-camphor R-butynol complex at 1 Kelvin.

An experimental spectrum is likely to have more than one species present, including impurities, conformations, complexes, and isotopologues. These added species result in a more complex experimental spectrum. Additionally, analytes can have multiple low energy conformers that can be observed experimentally. The conformation of a molecule is dependent on the dihedral angles of rotation around a bond and alters the mass distribution. These conformations result in different rotational constants and, therefore, different spectra can be seen in an experimental spectrum. The experimental spectrum has high resolution with little overlap, which makes it perfect for identifying different peak transitions, allowing mixture analysis.[15]

II. Structural Identification

While comparing the experimental rotational constants to the theoretical constants spectral comparison does provide a result for the molecule in the sample, there is a "gold standard" method of structure determination by identifying ^{13}C singly-substituted isotopologues in natural abundance in comparison to theory. By running the experiment for longer, the isotopologues can be detected in their natural abundance by driving down the noise.[16] This can require a much larger amount of sample and measurement time as the isotopologues are in much less abundance. 13-carbon, observed as it is a stable isotope, occurs at approximately 1% in natural abundance. This 1% abundance results in signal levels 1% the intensity of the parent species. However, it provides the distinct spectra for each of the isotopologues. The rotational constants found from the isotopologues are utilized in a Kraitchman analysis to build the structure of the molecule atom by atom.[17] This is done by solving for the moments of inertia and then using those to calculate the location of the substituted atom with regards to the initial molecule's center of mass. This is represented by equation 5 for $I_{xx'}$.

$$I_{xx'} = I_x + \Delta m(y^2 + z^2) - \frac{(\Delta my)^2}{M+\Delta m} - \frac{(\Delta mz)^2}{M+\Delta m} = I_x + \mu(y^2 + z^2) \quad (5)$$

Where Ix is the principal moment of inertia, M is the mass of the original molecule, Δm is the difference in mass of the original and substituted molecules, μ is equal to M*Δm / M+Δm and the coordinates of the substituted atom in reference to the original molecules center of mass are x, y and z. The coordinates of each atom can be solved for by obtaining all of the isotopologues. This provides the structure of the molecule in question with X-ray diffraction quality.[18]

III. Microwave Spectrometers

With the research into microwave radar technology during World War II, the ground work was laid for technical advancement.[19] The initial spectrometers utilized after the war were wave guide absorption spectrometers, seen in Figure 2.

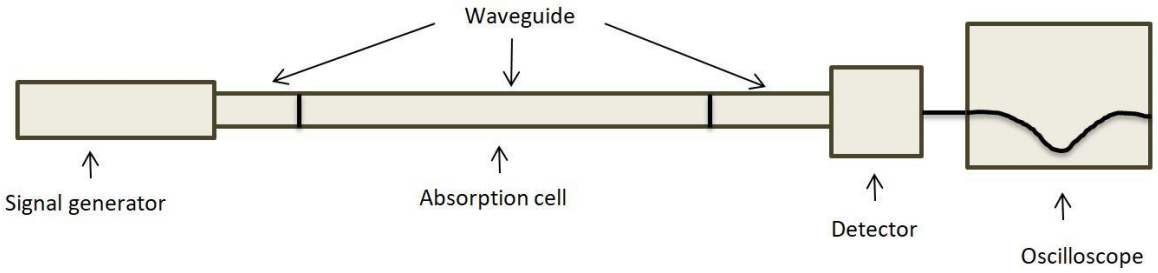

Figure 2: An absorption waveguide spectrometer

These spectrometers were composed of a signal generator connected to a metal tube (the wave guide). A portion of the wave guide is contained within two mica windows, known as the absorption cell. Gas molecules are trapped inside of the absorption cell and have microwave radiation sent through them. On one end of the waveguide, a detector registers the decrease in microwave radiation when the microwave frequency matches an absorption frequency of the molecule.[12, 20-22] This decrease can be seen on an oscilloscope. The absorption wave guide spectrometer had the issue that the gas was at room temperature, which results in a larger distribution of energy levels. As the intensity of a transition is dependent on the population of the energy levels, this limits the sensitivity of the measurement. This technique, while providing the absorption spectrum of a gas, was later improved through the use of a Sark field.[23-24] By applying an electric field to a gas, the population of energy levels changes and the dipole moment is solved for.[12, 25] However, this still did not account for the room temperature measurement. To

address this issue, a pulsed jet system was implemented. The pulsed jet relies on the expansion of a gas through a small aperture, creating a supersonic expansion. This expansion converts thermal translational energy into directed directional velocity.[26] The decreasing of this thermal energy resulted in less degrees of freedom of rotational and vibrational degrees of freedom, thus reducing the number of populated states.[27] This is seen through the correlation of temperature to the rotational partition function in equation 6 and related back to equation 2.

$$z_{rot} = \sum_{J=0}^{\infty}(2J+1)e^{-\left(\frac{\Theta_{rot}}{T}\right)J(J+1)}, \quad \Theta_{rot} \equiv \frac{\hbar^2}{2Ik} \tag{6}$$

Where J is the energy level, T is temperature, Θ_{rot} is the characteristic rotational temperature based on the moment of inertia (I), Boltzmann's constant (k) and the reduced Pank's constant ($\hbar$). As the temperature decreases, the rotational partition function gets smaller. The Boltzmann distribution then shifts in favor of the molecular state with a lower energy. This significantly simplifies the number of transitions observed in microwave spectroscopy. While the concept of the jet pulse expansion was discussed and used in fluorescence excitation in 1975, it was not used in microwave spectroscopy until the mid-1990's.[26-27] One difficulty with these early spectrometers was that they functioned in the frequency domain, limiting the sensitivity. To improve sensitivity, Fourier transform (FT) spectrometers were developed to measure the signal in the time domain.[6] The FT spectrometer relied on exciting the sample and measuring the free induction decay (FID). This removed the noise related to the microwave radiation source, as well as averaging the signals, which averages out any remaining noise. Shortly after the use of Fourier transform technology in microwave spectrometers, another advance was made in 1979. This advance involved the combination of the Fourier transform, jet pulse technology, and a Fabry-Perot resonance cavity as the absorption cell. The Fabry-Perot resonance cavity had been used

before as an absorption cell prior to the use of the Fourier transform and jet pulse.[28] However, this was the first spectrometer that utilized all three of these techniques in concert, and therefore was referred to as a Balle-Flygare spectrometer.[7, 29] The Fabry-Perot cavity has a higher quality factor then traditional absorption cells, increasing the sensitivity of the instrument:[28]

$$(\gamma)_{min} = \left(\frac{4kTN\Delta f}{P_0}\right)^{\frac{1}{2}} \left(\frac{2\pi}{Q_L \lambda}\right) \quad (7)$$

This equation relates the coefficient of absorption (γ) to the Q factor (Q_L), as well as temperature (T), Boltzmann's constant (k), noise (N), bandwidth (Δf), wavelength (λ) and the microwave power (P_o). Specifically, it's seen that as the Q factor increases, the minimum absorption signal that the instrument can detect decreases. By combining the three different techniques, the Balle-Flygare spectrometer had a better sensitivity than the previous iterations of microwave spectrometers.[7, 29-30] This, along with its high resolution, made it the preferred microwave spectrometer for many years and is still used today.[31-33] While the increase in sensitivity and the high resolution of this spectrometer made it widely used, it was limited in the time it took to perform a measurement. To measure a large frequency range, or broadband measurement, the instrument has to measure many separate frequency ranges in a step wise method. A measurement using this instrument could take 14 hours to collect an 11 GHz range, limiting the usefulness of microwave spectroscopy.[9] The benefit to running a broadband measurement provides a larger number of transitions over a greater frequency range. This provides better determination of different molecules in a mixture due to different frequency ranges for peak transitions.

In order to achieve a faster broadband measurement, the Pate group designed a chirped-pulse Fourier transform microwave spectrometer (CP-FTMW).[9] A chirped-pulse is a pulse of

radiation that covers a linear frequency range in a μs time frame.[34] This improvement used newer waveform generators and digitizers that covered an entire 11GHz frequency range.[9, 35] This shortened the time span of microwave experiments by 40% compared to the Balle-Flygare spectrometer, and it also resulted in less sample required for the measurement. Further advances were found to decrease this time by 90%, and sample consumption by 30%.[9] The broadband capability and the fast measurement time allowed for the measurement of μs length reactions.[36] Due to the advances in digital electronics, the frequency range that could be covered was increased, in some cases it covered 30-60 GHz, allowing for the detection of many transitions.[37-38] The improvements in sensitivity, sample consumption, and measurement time have made it possible to measure samples with low signal levels in a reasonable amount of time. As such, different compounds complexing with each other can be investigated, allowing for the chiral tag technique to function for absolute configuration determination.

IV. Quantum Theory Calculations

An important component of rotational spectroscopy is the computational methods and calculations. Computational methods have gone through periods of improvement and optimization for different accuracy and computational requirements.[39] Two of the main computational methods are second order Møller-Plesset (MP2) perturbation theory and density functional theory (DFT).[40] The MP theory includes electron correlation in Hartree-Fock methods, whereas DFT uses the electron density to solve for the ground state energy.[41-44] MP2 is generally computationally intense, while DFT methods can provide faster computation times.[45] The methods used in the measurements discussed later require accurate structure computations. The optimal methods provide the necessary accuracy without high computational requirements. The B3LYP D3BJ method, a DFT method, was shown to have less computational requirements

then MP2 while still providing accurate structure.[40, 45] The basis set def2-TZVP was chosen for the calculations as it had previously been shown to give good complex structures over basis set 6-311++G(d,p).[46-49]

The accuracy of computational chemistry allows rotational spectroscopy to function as a library free identification system. This is due to the fact that theoretical rotational constants can be directly compared to experimental rotational constants. Paired with the intrinsic high resolution of this technique, this allows complex mixture analysis with identification of unknown species in the spectrum.

References

1. Guirgis, G. A.; Overby, J. S.; Palmer, M. H.; Peebles, R. A.; Peebles, S. A.; Elmuti, L. F.; Obenchain, D. A.; Pate, B. H.; Seifert, N. A., Molecular Structure of Methyldifluoroisocyanato Silane: A Combined Microwave Spectral and Theoretical Study. *J. Phys. Chem. A* **2012,** *116* (30), 7822-7829.
2. Schwoch, D., A complete molecular structure determination of pentaborane(9) by rotational spectroscopy. *Inorganic chemistry* **1977,** *16* (12), 3219-3222.
3. Steber, A. L.; Neill, J. L.; Zaleski, D. P.; Pate, B. H.; Lesarri, A.; Bird, R. G.; Vaquero-Vara, V.; Pratt, D. W., Structural studies of biomolecules in the gas phase by chirped-pulse Fourier transform microwave spectroscopy. *Faraday Discussions* **2011,** *150* (0), 227-242.
4. Wilson, E. B., Microwave Spectroscopy in Chemistry. *Science* **1968,** *162* (3849), 59.
5. Cleeton, C. E.; Williams, N. H., Electromagnetic Waves of 1.1 cm Wave-Length and the Absorption Spectrum of Ammonia. *Physical Review* **1934,** *45* (4), 234-237.
6. Ekkers, J.; Flygare, W. H., Pulsed microwave Fourier transform spectrometer. *Review of Scientific Instruments* **1976,** *47* (4), 448-454.
7. Balle, T. J.; Flygare, W. H., Fabry–Perot cavity pulsed Fourier transform microwave spectrometer with a pulsed nozzle particle source. *Review of Scientific Instruments* **1981,** *52* (1), 33-45.
8. Grabow, J.-U.; Palmer, E. S.; McCarthy, M. C.; Thaddeus, P., Supersonic-jet cryogenic-resonator coaxially oriented beam-resonator arrangement Fourier transform microwave spectrometer. *Review of Scientific Instruments* **2005,** *76* (9), 093106.
9. Brown, G. G.; Dian, B. C.; Douglass, K. O.; Geyer, S. M.; Shipman, S. T.; Pate, B. H., A broadband Fourier transform microwave spectrometer based on chirped pulse excitation. *Rev. Sci. Instrum.* **2008,** *79* (5), 053103/1-053103/13.
10. Seifert, N. A.; Perez, C.; Neill, J. L.; Pate, B. H.; Vallejo-Lopez, M.; Lesarri, A.; Cocinero, E. J.; Castano, F., Chiral recognition and atropisomerism in the sevoflurane dimer. *Phys. Chem. Chem. Phys.* **2015,** *17* (28), 18282-18287.
11. Patterson, D.; Schnell, M.; Doyle, J. M., Enantiomer-specific detection of chiral molecules via microwave spectroscopy. *Nature* **2013,** *497* (7450), 475-7.
12. Levine, I. N., *Physical Chemistry*. 5th ed.; McGraw-Hill: New York, 2002.
13. Bernath, P., *Spectra of Atome and Molecules*. Third ed.; Oxfod University Press: New York, NY, 2016; p 465.
14. C.H. Townes, A. L. S., *Microwave Spectroscopy*. Dover Publications: New York, N.Y,, 1975.
15. Gordy, W., Cook, R., Microwave Molecular Spectra. 3rd ed.; Knovel: 1984.
16. Brandon Carroll, P.; McGuire, B. A.; Zaleski, D. P.; Neill, J. L.; Pate, B. H.; Widicus Weaver, S. L., The pure rotational spectrum of glycolaldehyde isotopologues observed in natural abundance. *J. Mol. Spectrosc.* **2013,** *284-285*, 21-28.
17. Kraitchman, J., Determination of Molecular Structure from Microwave Spectroscopic Data. *American Journal of Physics* **1953,** *21* (1), 17-24.
18. Shipman, S. T.; Neill, J. L.; Suenram, R. D.; Muckle, M. T.; Pate, B. H., Structure Determination of Strawberry Aldehyde by Broadband Microwave Spectroscopy: Conformational Stabilization by Dispersive Interactions. *J. Phys. Chem. Lett.* **2011,** *2* (5), 443-448.
19. Walter Gordy, W. S., Ralph Trambarulo, *Micro-Wave Spectroscopy*. Dover Publications: New York, N.Y., 1966.
20. Hershberger, W. D., The Absorption of Microwaves by Gases. *Journal of Applied Physics* **1946,** *17* (6), 495-500.
21. Southworth, G. C., Hyper-frequency wave guides — General considerations and experimental results. *The Bell System Technical Journal* **1936,** *15* (2), 284-309.

22. Townes, C. H., The Ammonia Spectrum and Line Shapes Near 1.25-cm Wave-Length. *Physical Review* **1946,** *70* (9-10), 665-671.
23. Hughes, R. H.; Wilson, E. B., A Microwave Spectrograph. *Physical Review* **1947,** *71* (8), 562-563.
24. McAfee, K. B.; Hughes, R. H.; Wilson, E. B., A Stark-Effect Microwave Spectrograph of High Sensitivity. *Review of Scientific Instruments* **1949,** *20* (11), 821-826.
25. Jang, H.; Ka, S.; Peebles, S. A.; Peebles, R. A.; Oh, J. J., Microwave spectrum, structure and dipole moment of 3-fluorophenylacetylene (3FPA). *Journal of Molecular Structure* **2016,** *1125*, 405-412.
26. Smalley, R. E.; Wharton, L.; Levy, D. H., The fluorescence excitation spectrum of rotationally cooled NO2. *The Journal of Chemical Physics* **1975,** *63* (11), 4977-4989.
27. Melandri, S.; Caminati, W.; Favero, L. B.; Millemaggi, A.; Favero, P. G., A microwave free jet absorption spectrometer and its first applications. *Journal of Molecular Structure* **1995,** *352-353*, 253-258.
28. Hrubesh, L. W.; Anderson, R. E.; Rinehart, E. A., A Cavity Search Spectrometer for Free Radical Microwave Rotational Absorption Studies. *Review of Scientific Instruments* **1971,** *42* (6), 789-796.
29. Balle, T. J.; Campbell, E. J.; Keenan, M. R.; Flygare, W. H., A new method for observing the rotational spectra of weak molecular complexes: KrHCl. *The Journal of Chemical Physics* **1980,** *72* (2), 922-932.
30. Campbell, E. J.; Buxton, L. W.; Balle, T. J.; Flygare, W. H., The theory of pulsed Fourier transform microwave spectroscopy carried out in a Fabry–Perot cavity: Static gas. *The Journal of Chemical Physics* **1981,** *74* (2), 813-828.
31. Arunan, E.; Gutowsky, H. S., The rotational spectrum, structure and dynamics of a benzene dimer. *The Journal of Chemical Physics* **1993,** *98* (5), 4294-4296.
32. Indris, O.; Stahl, W.; Kretschmer, U., The Molecular Structure of Morpholine and the Morpholine–H2O Complex Determined by FT Microwave Spectroscopy. *Journal of Molecular Spectroscopy* **1998,** *190* (2), 372-378.
33. Leung, H. O.; Marshall, M. D.; Messinger, J. P.; Knowlton, G. S.; Sundheim, K. M.; Cheung-Lau, J. C., The microwave spectra and molecular structures of 2-chloro-1,1-difluoroethylene and its complex with the argon atom. *Journal of Molecular Spectroscopy* **2014,** *305*, 25-33.
34. Treacy, E. B., CHIRPED OPTICAL PULSES*. *Annals of the New York Academy of Sciences* **1969,** *168* (3), 400-418.
35. Brown, G. G.; Dian, B. C.; Douglass, K. O.; Geyer, S. M.; Pate, B. H., The rotational spectrum of epifluorohydrin measured by chirped-pulse Fourier transform microwave spectroscopy. *J. Mol. Spectrosc.* **2006,** *238* (2), 200-212.
36. Abeysekera, C.; Zack, L. N.; Park, G. B.; Joalland, B.; Oldham, J. M.; Prozument, K.; Ariyasingha, N. M.; Sims, I. R.; Field, R. W.; Suits, A. G., A chirped-pulse Fourier-transform microwave/pulsed uniform flow spectrometer. II. Performance and applications for reaction dynamics. *The Journal of Chemical Physics* **2014,** *141* (21), 214203.
37. Neill, J. L.; Harris, B. J.; Steber, A. L.; Douglass, K. O.; Plusquellic, D. F.; Pate, B. H., Segmented chirped-pulse Fourier transform submillimeter spectroscopy for broadband gas analysis. *Opt Express* **2013,** *21* (17), 19743-9.
38. Steber, A. L.; Harris, B. J.; Neill, J. L.; Pate, B. H., An arbitrary waveform generator based chirped pulse Fourier transform spectrometer operating from 260 to 295 GHz. *J. Mol. Spectrosc.* **2012,** *280*, 3-10.
39. Puzzarini, C.; Stanton, J. F.; Gauss, J., Quantum-chemical calculation of spectroscopic parameters for rotational spectroscopy. *International Reviews in Physical Chemistry* **2010,** *29* (2), 273-367.
40. Marshall, F. E.; Sedo, G.; West, C.; Pate, B. H.; Allpress, S. M.; Evans, C. J.; Godfrey, P. D.; McNaughton, D.; Grubbs, G. S., The rotational spectrum and complete heavy atom structure of the chiral molecule verbenone. *Journal of Molecular Spectroscopy* **2017,** *342*, 109-115.

41. Dyall, K. G., Second-order Møller-Plesset perturbation theory for molecular Dirac-Hartree-Fock wavefunctions. Theory for up to two open-shell electrons. *Chemical Physics Letters* **1994,** *224* (1), 186-194.
42. Hohenberg, P. C.; Kohn, W.; Sham, L. J., The Beginnings and Some Thoughts on the Future. In *Advances in Quantum Chemistry*, Löwdin, P.-O., Ed. Academic Press: 1990; Vol. 21, pp 7-26.
43. Hohenberg, P.; Kohn, W., Inhomogeneous Electron Gas. *Physical Review* **1964,** *136* (3B), B864-B871.
44. Kohn, W.; Sham, L. J., Self-Consistent Equations Including Exchange and Correlation Effects. *Physical Review* **1965,** *140* (4A), A1133-A1138.
45. Grimme, S.; Steinmetz, M., Effects of London dispersion correction in density functional theory on the structures of organic molecules in the gas phase. *Physical Chemistry Chemical Physics* **2013,** *15* (38), 16031-16042.
46. Weigend, F.; Ahlrichs, R., Balanced basis sets of split valence, triple zeta valence and quadruple zeta valence quality for H to Rn: Design and assessment of accuracy. *Physical Chemistry Chemical Physics* **2005,** *7* (18), 3297-3305.
47. Krishnan, R.; Binkley, J. S.; Seeger, R.; Pople, J. A., Self-consistent molecular orbital methods. XX. A basis set for correlated wave functions. *The Journal of Chemical Physics* **1980,** *72* (1), 650-654.
48. Glukhovtsev, M. N.; Pross, A.; McGrath, M. P.; Radom, L., Extension of Gaussian-2 (G2) theory to bromine- and iodine-containing molecules: Use of effective core potentials. *The Journal of Chemical Physics* **1995,** *103* (5), 1878-1885.
49. Curtiss, L. A.; McGrath, M. P.; Blaudeau, J. P.; Davis, N. E.; Binning, R. C.; Radom, L., Extension of Gaussian-2 theory to molecules containing third-row atoms Ga–Kr. *The Journal of Chemical Physics* **1995,** *103* (14), 6104-6113.

Chapter 2

Enantiomeric Analysis

I. Chirality

Chirality must be discussed to understand why rotational spectroscopy has previously been unable to function on enantiomers. Chirality originates from an atom that is connected to four different substitutents.[1] The chiral center, as defined by IUPAC, is an "atom holding a set of ligands in a spatial arrangement that is not superimposable on its mirror image."[2] The enantiomers, mirror image compounds, are the same structurally, but function differently in a chiral environment. As the number of chiral centers increases, the number of diastereomers increases by 2^{N-1} per chiral center (N). Rotational spectroscopy has already been discussed to have high resolution and, therefore, functions well for diastereomer analysis due to the unique geometries of diastereomers resulting in unique rotational spectra. However, the number of enantiomers also increases, and being able to identify enantiomers is necessary for chiral analysis. For the enantiomeric side of chiral analysis, there are two challenges: the absolute configuration (AC) determination, and the enantiomeric excess (ee) determination. This thesis focuses on absolute configuration determination by rotational spectroscopy.

These enantiomers have the same physical properties and act the same in an achiral environment, but have different optical rotations (an asymmetric rotation of plane polarized light through different enantiomers), and different actions in chiral environments.[3] This structural similarity makes it impossible for traditional rotational spectroscopy to distinguish the enantiomers from each other because they have mirror image mass distributions, therefore, resulting in the same rotational constants and rotational spectra. While rotational spectroscopy has been limited to diastereomer analysis, there are other techniques that have been used for chiral analysis.[4]

II. Current Techniques

Louis Pasteur introduced the concept of chirality with the separation of optical isomers to chemistry in 1848.[5] Now, chirality plays an important role in the pharmaceutical industry. A paper in 2002 estimated that 56% of drugs were chiral compounds.[6] Due to this large number of chiral compounds in use, techniques had to be developed for the detection and analysis of chiral molecules. Pasteur first saw this difference using optical activity, the rotation of polarized light passed through a solution of the compounds.[7] This discovery lead to the development of many techniques for the detection and analysis of diastereomers and enantiomers. The isomers that are optically active have a specific rotation used to identify the isomer. This specific rotation for an optically active substance, B, is defined as:

$$[\alpha]_\lambda \equiv \frac{\alpha_\lambda}{[\rho_B/\left(\frac{g}{cm^3}\right)](\frac{l}{dm})} \tag{2.1}$$

where α_λ is the angle of optical rotation, ρ_B is the mass concentration of B, and l is the path length. [8] This specific rotation provides the isomers with either a clock-wise rotation, (positive $[\alpha]_\lambda$) known as dextrorotary, or a counter clock-wise rotation, (negative $[\alpha]_\lambda$) known as levorotatory. The difference in rotation provides the absolute configuration of the molecule in question. Circular dichroism methods are another group of techniques that utilize differential interaction of light based on molecular structure.

Circular dichroism (CD) is the difference in absorption of left and right circularly polarized radiation in chiral molecules and is equal but opposite for enantiomers.[9] This is measured in CD instruments as shown by equation 2.2 and how it can be converted to the molar circular dichroism in equation 2.3.

$$\Delta A = A_L - A_R \quad (2.2)$$

$$\Delta \varepsilon = \varepsilon_L - \varepsilon_R = (A_L - A_R)/cl \quad (2.3)$$

Where A_L is the absorption of left circularly polarized light, A_R is the absorption of the right circularly polarized light, ε_L is the molar extinction coefficient for left polarized light, ε_R is the molar extinction coefficient for right polarized light, c is the concentration of the sample and *l* is the sample thickness or path length.[10] Circular dichroism is essentially a blanket term covering several different techniques; under this there is electronic circular dichroism, vibrational circular dichroism and photoelectron circular dichroism, to name a few. These techniques can be used as a technique for absolute determination or conformational analysis of macromolecules.[11]

Electronic circular dichroism (ECD) measurements are performed in the visible and ultraviolet regions of light which provide insight on electronic transitions. It has been used for conformational analysis of biomolecules and for absolute configuration determination.[12] The difficulty with ECD is that it does require a chromophore to be present in the molecule. The more recent technique of vibrational circular dichroism (VCD) is built on the same basis, however, utilizes absorption in the infrared region of light. This is considered to be easier than ECD due to the prevalence of chromophores in the infrared region.[9, 11] VCD is finding use for absolute configuration determination as well as enantiomeric excess determination.[13] To determine the AC for a molecule, the experimental IR spectrum is obtained for a known enantiomer, and the conformations of the molecule must be calculated for room temperature conditions. The theoretical VCD spectra of these conformations are then calculated, weighted, and summed to get the average VCD spectrum. The experimental spectrum is obtained by using circularly polarized light in both left and right polarizations; the absorption is then obtained for

both polarizations independently and a difference calculated. This leads to direct comparison of the theoretical VCD spectrum to that of the experimental.[14] Photoelectron circular dichroism (PECD), while once again relying on the difference in absorbance of left and right circularly polarized light, is based on the photoelectron angular scattering distribution upon ionization.[15] For PECD, the molecule of interest is photoionized by circularly polarized light. After this ionization, the distribution of photoelectrons is recorded, which is different for enantiomers.[16-17] These are some of the main circular dichroism techniques used to identify enantiomers. However, there are some downsides to these methods. VCD and CD obtain no signal for a racemic sample, making measurements on mixtures that are close to being racemic difficult nor do these methods function well in complex mixtures with already low signal levels.[18] VCD and CD also rely on the interactions of the electric dipole and the magnetic dipole transition moments, which are intrinsically weak and result in lower signals.[19-20] PECD on the other hand relies on mass spectrometry for molecule identification in mixtures. This reliance can make identification difficult if there are similar size molecules in the sample.

While these provide spectroscopic methods of absolute configuration determination, there is also the use of chiral chromatography. Chromatography as a technique has been around since the early 1900's and has seen many advancements since its inception.[21] Due to its capability in separating compounds, its use was investigated and extended to chiral molecules.[4, 22-23] Just like there are different kinds of circular dichroism, there are different methods of chromatography. For example, liquid chromatography as well as gas chromatography, has been used for chiral separation and detection.[4, 23-24] These techniques function as a separation technique, unlike the previous methods, however, rely on another method for identifying unknowns. The basis of chromatography is the difference in affinity for the solid phase of the

column. The enantiomers will elute at different rates from the column based on which one has less of an affinity for the column.[21] However, it can require chiral derivatization as well as testing to know which enantiomer will elute first. As discussed in the previous chapter, rotational spectroscopy is the technique being investigated in this thesis. As such, it is necessary to discuss a more recent method of microwave three-wave mixing for absolute configuration determination.

Three-wave mixing is a rotational spectroscopy method that relies on the fact that enantiomers have a dipole moment component from the electric dipole moment projected onto the principal axis system that is equal but opposite. While they have two dipole components that are the same sign and magnitude, the scalar triple product (μ_a x μ_b • μ_c) of all three will have an opposite sign between enantiomers.[25] This provides a means of measuring absolute configuration with rotational spectroscopy. The ability comes from the 180° difference in phase for the collected FID between enantiomers, which acts as a chiral signal.[25-27] The measurement is performed by using a three horn set-up with mutually orthogonal polarization. The first pulse duration of polarized light is optimized to fit a pi/2 pulse and creates coherence, while the second pulse duration is optimized to fit a pi pulse to transfer coherence as a function of pulse duration. These excite the molecule based upon the targeted a-, b-, or c- type transition. The detection horn detects the signal which is the same amplitude and frequency between enantiomers, however, it is completely out of phase. Currently, this requires a reference sample to determine the absolute configuration. The method presented here is a rotational spectroscopy technique like three-wave mixing. However, it uses current methods unlike the aforementioned.

III. Chiral Tag Rotational Spectroscopy

As mentioned in the previous chapter, traditional rotational spectroscopy does not work for enantiomers due to the mirror image mass distributions. Due to this issue, rotational

spectroscopy has been limited to identifying diastereomers. Chiral tag rotational spectroscopy relies on the ability of a chiral molecule to complex with another chiral molecule by van der Waals attractions or other intermolecular forces in a pulsed jet expansion.[28-29] For instance, when an R enantiomer is complexed with another R-enantiomer it will form a homochiral complex. This naming scheme takes into account only one chiral center, when more chiral centers are present, it is advantageous to use (+)/(-) nomenclature. When the R enantiomer complexes with an S-enantiomer it will form a heterochiral complex. These homo- and heterochiral complexes, while being composed of molecules that are indistinguishable by rotational spectroscopy, form complexes that are distinguishable because of different distributions of mass, therefore observing different rotational spectra.

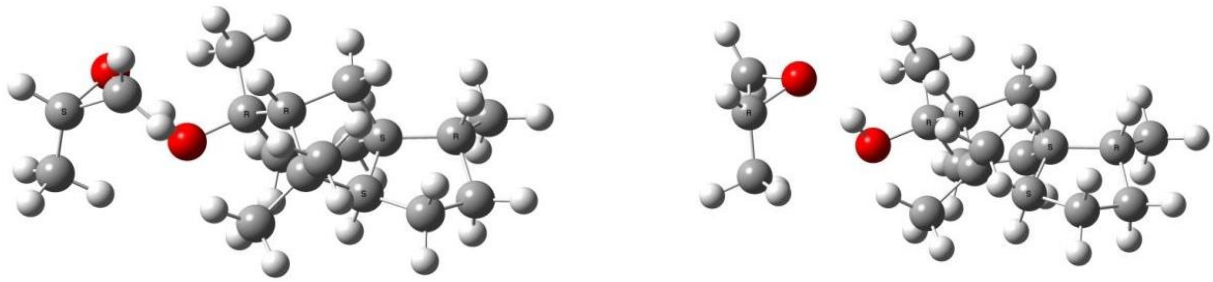

Figure 2.1: (+) cedrol complexed with (*S*)-propylene oxide (left) and (*R*)-propylene oxide (right)

The (+)-cedrol can be seen in Figure 2.1 complexing differently with the (*S*)- and (*R*)-propylene oxide. The two different complexes both have cedrol in the same orientation while the propylene oxide has a different orientation dependent on how it is complexing with the cedrol as shown in the figure. While before the complexation the (*S*)- and (*R*)-propylene oxide had mirror image mass distributions, they now have different mass distributions due to the difference in propylene oxide orientation and atom location. As this is the basis of rotational constants, the difference can be seen in Table 2.1.

Table 2.1: The rotational constants and dipole moment components of a (+) cedrol (*S*)-propylene oxide complex and a (+) cedrol (*R*)-propylene oxide complex.

Parameter	(+) cedrol (*S*)-propylene oxide	(+) cedrol (*R*)-propylene oxide
A/MHz	684.69	698.1
B/MHz	201.24	193.6
C/MHz	180.15	172.0
μ_a/D	-1.44	2.3
μ_b/D	-1.49	0.1
μ_c/D	0.90	0.3

These complexes show different rotational constants as well as different dipole moments. The difference in rotational constants and the use of the dipole moments will be discussed in a later chapter.

These complexes are not the only potential complex of these molecules. Within the pulsed jet gas expansion, many rotational states may be occupied. However, the lower rotational temperatures from this sample introduction minimizes the complexity. Figure 2.2 shows how close or far energy levels can be for the isomers, which affects the abundance of those forms in the experimental spectrum. The energies for these complexes are relative to the lowest energy, which is designated by the 0.00 kcal/mol complex. The calculated energy levels of the complexes varies based on what theory the calculations are performed at, with B3LYP D3BJ having been selected as it provides reliable structures with less computational cost than MP2; the def2-tzvp basis set is also chosen as it gives better complex structures than other basis sets.[28]

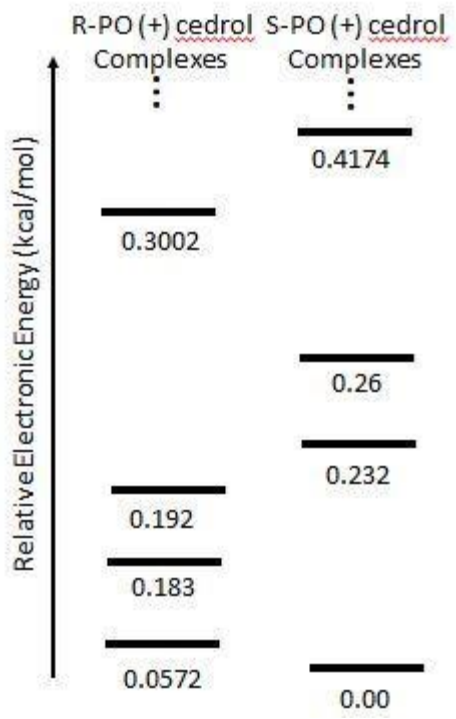

Figure 2.2: The relative energies of four complexes for both (*R*)-propylene oxide (+) cedrol and (*S*)-propylene oxide (+) cedrol

From the list of calculated complexes, there are normally several lower energy conformations which are clustered around lower energies and higher energies clustered around larger energy gaps. The lower energy complexes are expected to be the most abundant in the experiment due to the adiabatic expansion rotationally cooling the molecules. This does not mean that the other complexes will not be present, but that they will be much less abundant. These complexes are compared to the experimental species by the traditional method of rotational constant comparison. There are further methods of verification that can be used if the rotational constant comparison is not accurate enough. These include the potential for dipole comparison or Kraitchman substitution, discussed in the first chapter.

References

1. Tro, N. J., *Chemistry Structure and Properties*. Second ed.; Pearson education: New York, NY, 2018.
2. L.G. Wade, J., *Organic Chemistry*. Eighth ed.; Pearson education: New York, NY, 2013.
3. Francis A. Carey, R. L. S., *Advanced Organic Chemistry Part A: Structure and Mechanisms*. Fifth Edition ed.; Springer: 2007.
4. Ward, T. J.; Hamburg, D. M., Chiral separations. *Analytical Chemistry* **2004,** *76* (16), 4635-4644.
5. Lien Ai Nguyen, H. H., Chuong Pham-Huy, Chiral Drugs An Overview. *International journal of Biomedical science* **2006**.
6. Rentsch, K. M., The importance of stereoselective determination of drugs in the clinical laboratory. *Journal of Biochemical and Biophysical Methods* **2002,** *54* (1), 1-9.
7. Mauskopf, S., CHAPTER 1 - A history of chirality. In *Chiral Analysis*, Busch, K. W.; Busch, M. A., Eds. Elsevier: Amsterdam, 2006; pp 3-24.
8. Levine, I. N., *Physical Chemistry*. 5th ed.; McGraw-Hill: New York, 2002.
9. Stephens, P. J., Theory of vibrational circular dichroism. *The Journal of Physical Chemistry* **1985,** *89* (5), 748-752.
10. Woody, R. W., [4] Circular dichroism. In *Methods in Enzymology*, Academic Press: 1995; Vol. 246, pp 34-71.
11. Di Bari, L.; Pescitelli, G., Electronic Circular Dichroism. *Computational Spectroscopy* **2010**.
12. *Circular Dichroism and the Conformational Analysis of Biomolecules*. Plenum Press: 1996.
13. Nafie, L. A.; Long, F.; Freedman, T. B.; Buijs, H.; Rilling, A.; Roy, J.-R.; Dukor, R. K., The determination of enantiomeric purity and absolute configuration by vibrational circular dichroism spectroscopy. *AIP Conference Proceedings* **1998,** *430* (1), 432-434.
14. Stephens Philip, J.; Devlin Frank, J.; Pan, J.-J., The determination of the absolute configurations of chiral molecules using vibrational circular dichroism (VCD) spectroscopy. *Chirality* **2007,** *20* (5), 643-663.
15. Janssen, M. H.; Powis, I., Detecting chirality in molecules by imaging photoelectron circular dichroism. *Phys Chem Chem Phys* **2014,** *16* (3), 856-71.
16. Powis, I., Photoelectron Circular Dichroism. *Comprehensive Chiroptical Spectroscopy* **2012**.
17. Lux, C.; Wollenhaupt, M.; Bolze, T.; Liang, Q.; Köhler, J.; Sarpe, C.; Baumert, T., Circular Dichroism in the Photoelectron Angular Distributions of Camphor and Fenchone from Multiphoton Ionization with Femtosecond Laser Pulses. *Angewandte Chemie International Edition* **2012,** *51* (20), 5001-5005.
18. Cameron, R. P.; Götte, J. B.; Barnett, S. M., Chiral rotational spectroscopy. *Physical Review A* **2016,** *94* (3).
19. Patterson, D.; Schnell, M., New studies on molecular chirality in the gas phase: enantiomer differentiation and determination of enantiomeric excess. *Phys Chem Chem Phys* **2014,** *16* (23), 11114-23.
20. Domingos, S. R.; Perez, C.; Schnell, M., Sensing Chirality with Rotational Spectroscopy. *Annu Rev Phys Chem* **2018,** *69*, 499-519.
21. *Chromatography: A Laboratory Handbook of Chromatographic and Electrophoretic Methods*. Third Edition ed.; Van Nostrand Reinhold Company: New York, 1975.
22. Izake, E. L., Chiral discrimination and enantioselective analysis of drugs: an overview. *J Pharm Sci* **2007,** *96* (7), 1659-76.
23. Zhang, Y.; Wu, D.-R.; Wang-Iverson, D. B.; Tymiak, A. A., Enantioselective chromatography in drug discovery. *Drug Discovery Today* **2005,** *10* (8), 571-577.
24. Freissinet, C.; Buch, A.; Szopa, C.; Sternberg, R., Enantiomeric separation of volatile organics by gas chromatography for the in situ analysis of extraterrestrial materials: Kinetics and thermodynamics investigation of various chiral stationary phases. *Journal of Chromatography A* **2013,** *1306*, 59-71.

25. Lobsiger, S.; Perez, C.; Evangelisti, L.; Lehmann, K. K.; Pate, B. H., Molecular Structure and Chirality Detection by Fourier Transform Microwave Spectroscopy. *J. Phys. Chem. Lett.* **2015,** *6* (1), 196-200.
26. Eibenberger, S.; Doyle, J.; Patterson, D., Enantiomer-Specific State Transfer of Chiral Molecules. *Physical Review Letters* **2017,** *118* (12), 123002.
27. Patterson, D.; Schnell, M.; Doyle, J. M., Enantiomer-specific detection of chiral molecules via microwave spectroscopy. *Nature* **2013,** *497* (7450), 475-7.
28. Marshall, F. E.; Sedo, G.; West, C.; Pate, B. H.; Allpress, S. M.; Evans, C. J.; Godfrey, P. D.; McNaughton, D.; Grubbs, G. S., The rotational spectrum and complete heavy atom structure of the chiral molecule verbenone. *Journal of Molecular Spectroscopy* **2017,** *342*, 109-115.
29. Seifert, N. A.; Perez, C.; Neill, J. L.; Pate, B. H.; Vallejo-Lopez, M.; Lesarri, A.; Cocinero, E. J.; Castano, F., Chiral recognition and atropisomerism in the sevoflurane dimer. *Phys. Chem. Chem. Phys.* **2015,** *17* (28), 18282-18287.

Chapter 3

Enantiomeric Analysis of Camphor

I. Introduction

To test the ability of chiral tagging to correctly differentiate between enantiomers, the compound 1,7,7-trimethylbicyclo[2.2.1]heptan-2-one, better known as camphor, was chosen as a proof of principal experiment for absolute configuration determination. While camphor is a fairly large molecule in terms of rotational spectroscopy, 152.237 g/mol, the bicyclic ring structure results in a rigid molecule, which lowers the likelihood of a large number of conformational isomers. Camphor has been shown to have a small dipole moment along one of the principal axes by Kisiel *et al*.[1] Dipole moments are difficult to predict theoretically, and the direction of the small dipole component can be predicted incorrectly by theory if the dipole magnitude is small. If the direction of the dipole component is incorrectly predicted, the scalar triple product of the dipole components would be wrong, resulting in an erroneous absolute configuration determination by three-wave mixing. Also, while having two chiral centers, camphor is forced to be in the same configuration for both centers due to a bridge bond, as seen in Figure 3.1.

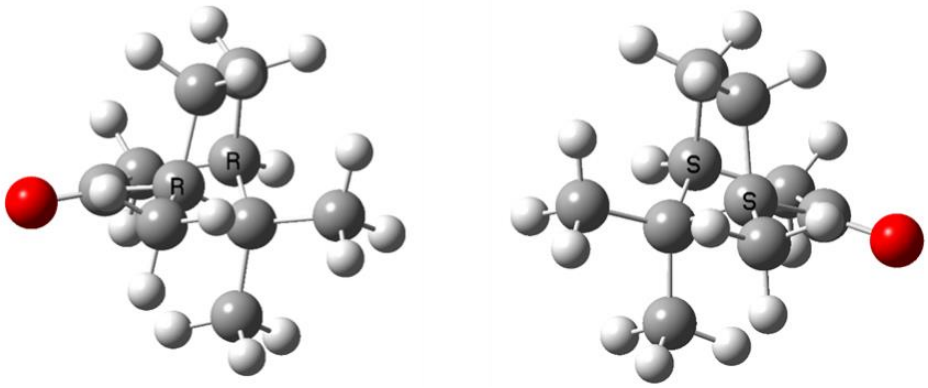

Figure 3.1: (+)-camphor (R-camphor) is shown on the left with (-)-camphor (S-camphor) on the right

As previously discussed, the number of isomers generally increases by 2^{n-1} for n chiral centers, however, this is not the case for camphor. The bridge formation, locking the two chiral centers into the same orientation, reduces the number of potential isomers that can be present in a sample of camphor. This decreases the spectral complexity when compared to other chiral compounds that do not have two bridged chiral centers. In the previous measurements by Kisiel *et al.,* the singly-substituted ^{13}C isotopologues were measured in natural abundance, allowing a Kraitchman analysis to be performed.[1] This ability allows the structure of camphor to be obtained and can be used to determine the carbon atom locations of the complexes in the pulsed jet such that you can build the structure atom by atom to accurately determine the absolute configuration of the analyte with gold standard quality.

II. Experimental

Optimized geometries of the camphor butynol complexes were predicted using Gaussian 09 Revision E.01 using the B3LYP D3BJ method and def2-tzvp basis set.[2-6] The use of this method and basis set has been discussed before.[7] To summarize, the best theoretical models need to be highly accurate when calculating complexes, however, the computational costs should be less than that of MP2 methods. As such, B3LYP D3BJ was selected as it provides reliable structures with less computational cost than MP2. The def2-tzvp basis set was selected as it gives better complex structures than other basis sets.[7-8] The lowest energy conformation of the camphor butynol complexes is shown in Figure 3.2 along with the rotational constants, dipole moments, and relative energies in Table 3.1.

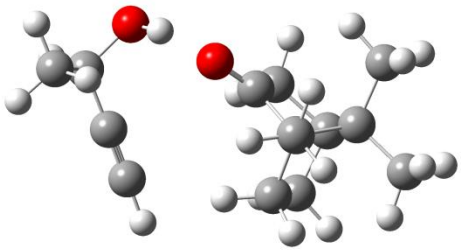

Figure 3.2. The calculated lowest energy conformational structure of the heterochiral camphor butynol complexes.

Table 3.1

Calculated structural parameters, dipole moment and energy of the lowest energy conformation for the camphor butynol complex.

Parameter	Value
A/MHz	975.3
B/MHz	320.1
C/MHz	301.6
μ_a/D	3.3
μ_b/D	1.6
μ_c/D	0.9
E/Hartree	-697.459468

This lowest energy complex for the heterochiral camphor butynol complex is expected to be the most abundant in the experimental spectrum.

To investigate the enantiomeric analysis of camphor by chiral tag rotational spectroscopy a tagging molecule had to be chosen. In this case (*R*)-3-btyn-2-ol and (*S*)-3-butyn-2-ol were chosen. Butynol is a small, rigid and cheap molecule that is utilized as a hydrogen bond donor being smaller than camphor by 70.09g/mol. The racemic and enantiopure forms were purchased from Sigma-Aldrich and used without further purification. A sample of butynol is placed in an external reservoir, and neon is flowed over this sample, entraining butynol in the neon carrier gas. Then, this gas mixture is, similarly, passed over the camphor sample. With the neon carrier gas now doped with butynol and camphor, pulsed-jet expansion of this mixture can result in molecular complexes of the tag and analyte. The pulsed-jet expansion occurs through a 1mm hole into a vacuum chamber of approximately 1.0E-5 Torr.

The experimental spectrum was collected on a chirped-pulse Fourier transform spectrometer that operates in the 2-8 GHz range. The set up used 5 solenoid valves to perform 5 simultaneous jet pulsed expansions at a 3 Hz repetition rate. For every gas pulse, 8 free induction decays (FID) were collected. (*R*)-Camphor (98%) was purchased from Sigma Aldrich® along with (*R*)-butynol (98%) and (*S*)-buyn-2-ol (97%). The racemic 3-Butyn-2-ol (>97.0%) (racemic

butynol) was purchased from Tokyo Chemical Industry CO. The samples were heated to approximately 50°C inside of the baseplate and then injected into the chamber.[9] The neon butynol gas mixtures at a pressure of ~15 psig. This gas mixture flowing over the camphor results in a 0.1% mixture of camphor in the gas.[10] The measurement that used (*R*)-butynol had 818 thousand FID averages taken, the (*S*)-butynol measurement had 1 million FID averages taken, and a racemic butynol measurement had 40 thousand FID averages taken. These FIDs are collected over multiple acquisitions, and then averaged over time to obtain the FID averages. The linewidth resolution for these measurements on this instrument has previously been shown to be 60 kHz.[7] The FID data was then Fourier transformed to obtain the data in the frequency domain. This data was then analyzed in JB95 to assign the experimental transition frequencies to the theoretical frequencies.[11]

III. Experimental Spectra and Analysis

The experimental spectrum for the racemic butynol complexed with camphor is shown in Figure 3.3. The a-type transitions were expected to have the strongest transitions as the dipole moment component for them was the largest. Quantum calculations suggested many low energy complexes of camphor/butynol would produce a-type dominant spectra. After frequencies were assigned, the experimental rotational constants were compared to the closest theoretical rotational constants seen in Table 3.2.

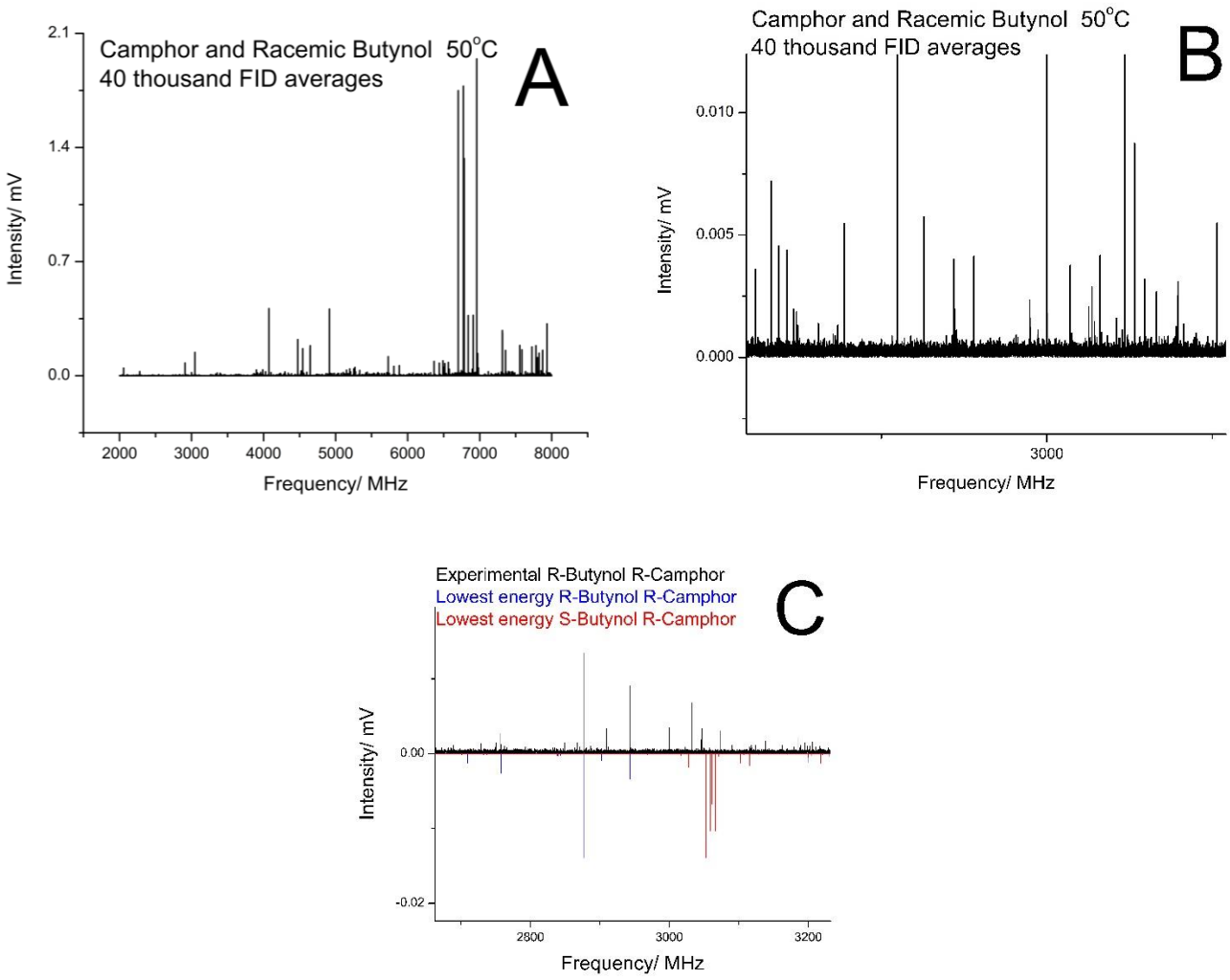

Fig. 3.3. Spectra of the camphor butynol complexes from 2-8 GHz. A shows the racemic butynol complexes with camphor spectrum from 40 thousand FID averages. B is a zoomed in section of the experimental spectrum in A. C is a comparison of the cut experimental (*R*)-butynol camphor spectrum to the simulated lowest energy homochiral and heterochiral complexes fitted from the racemic sample.

While the initial comparison was done visually by comparing the experimental spectra to the simulated spectra based on the quantum calculation, the more appropriate method was the comparison of theoretical and experimental rotational constants. The initial comparison shows that the lowest energy homochiral complex is a better match for the spectrum than the heterochiral lowest energy complex. The fitted quantum calculations are shown in Figure 3.3C, showing the presence of the lowest energy (*R*)-butynol (*R*)-camphor complex and lack of the lowest energy (*S*)-butynol (*R*)-camphor complex. For the rotational constant comparison, the

camphor sample was of a known enantiomer; therefore, the comparison was made with the appropriate theoretical calculations in mind. This meant the experimental spectrum of camphor with (*R*)-butynol was compared to the theoretical rotational constants of the camphor with (*R*)-butynol complex and not the camphor with (*S*)-butynol complex and vice versa. If the absolute configuration was unknown, then the complexes can be determined by cross comparing species due to the difference in rotational constants.

Table 3.2: A comparison of the experimental rotational constants and the closest theoretical conformations rotational constants.

Homochiral conformations (*R*)-camphor- (*R*) butynol				
Conformer	**Rotational constant A (MHz)**	**Rotational Constant B (MHz)**	**Rotational Constant C (MHz)**	**ΔE**
Experimental 1	1036.63867 (23)	291.898140 (63)	275.812670 (65)	…
Experimental 2	922.86399 (22)	307.166560 (74)	291.902210 (79)	…
Second lowest energy	923.3	312.1	296.19	56
Lowest energy	1038.6	294.6	278.5	18
Heterochiral conformations (*R*)-camphor- (*S*) butynol				
Conformer	**Rotational constant A (MHz)**	**Rotational Constant B (MHz)**	**Rotational Constant C (MHz)**	**ΔE**
Experimental 1	973.29413 (16)	314.891490 (96)	297.123310 (92)	…
Experimental 2	975.80396 (26)	286.505840 (71)	270.608750 (76)	…
Lowest energy	975.3	320.1	301.6	0*
Second lowest energy	977.7	290.8	274.2	56.1

*Absolute energy: -697.459468 Hartree

Looking at the rotational constants for the two lowest energy complexes for each family compared to the experimental rotational constants, there is good agreement between the matching constants. In the case of the highest intensity experimental homochiral species compared to the lowest energy homochiral complex, there are percent errors per rotational constant A, B, and C, of 0.19%, 0.93%, and 0.97%. These constants are much closer than the second lowest energy conformation with percent errors of 10.9%, 6.92%, and 7.39%. These errors show much better agreement for the lowest theoretical energy structure to the most abundant experimental species. This is also seen with the second most abundant experimental species. In this regard the second lowest theoretical energy structure has percent errors of 0.047%, 1.61%, and 1.47%. While the lowest energy theoretical structure had percent errors of

12.5%, 4.09%, and 4.81%. For further verification, the substitution structures by Kraitchman analysis for the homo and heterochiral families were obtained.

The ^{13}C isotopologues in natural abundance of the four most abundant species (2 for (*R*)-camphor (*R*)-butynol and 2 for (*R*)-camphor (*S*)-butynol) were analyzed to get the absolute structure of the complexes. These isotopologues signals were obtained from the two experimental spectra collected over 800 thousand averages. The most abundant species structures obtained from Kraitchman analysis are shown in Figure 3.4, while the coordinates of the substitution structure are listed in table 3.2, along with the experimental rotational constants. The structures show that the locations of the substituted atoms are in good agreement with the lowest theoretical energy structure with the highest Costain error for an atom position being 0.09 Å.

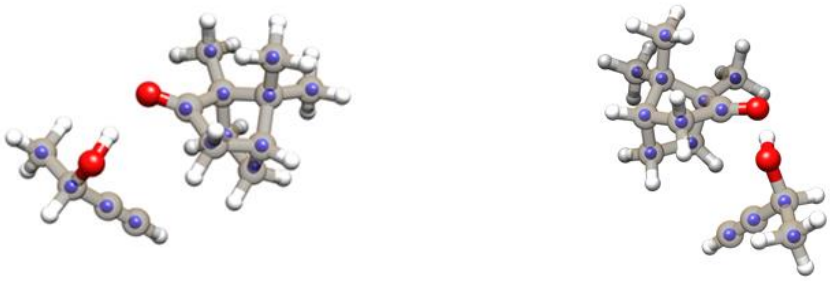

Most abundant heterochiral structure Most abundant homochiral structure

Fig. 3. The substitution structures for the two most abundant species of the camphor butynol complexes in the experimental spectra. The blue dots represent the locations of the atoms experimentally obtained by Kraitchman analysis within the theoretical parent structure.

Table 3.3: List of principal axis coordinates and rotational constants for Kraitchman analysis of the most abundant heterochiral complex

Atom-label number	*a*-coordinate Å	*b*-coordinate Å	*c*-coordinate Å	A/MHz	B/MHz	C/MHz
Carbon-2	0.15993(0.04377)[a]	0.67267(0.01041)	0[b]	972.474(51)	314.88922(24)	297.03993(25)
Carbon-3	1.45467(0.00365)	0.29832(0.01775)	0.76945(0.00693)	972.023(38)	314.36173(17)	296.73878(17)
Carbon-4	0.31812(0.02874)	0	-1.37149(0.00668)[c]	969.789(67)	314.50350(31)	297.10597(32)
Carbon-5	1.73523(0.00273)	1.25397(0.00367)	1.92965(0.00251)	963.504(33)	313.58838(15)	296.31332(16)
Carbon-6	1.67483(0.00357)	-0.84914(0.00698)	-1.1564(0.00523)	969.465(43)	314.08338(20)	296.50704(20)
Carbon-7	2.53302(0.00174)	0.10863(0.04083)	-0.32626(0.0136)	973.074(31)	313.61837(14)	296.00585(14)
Carbon-8	1.15345(0.00396)	-1.15458(0.00392)	1.18226(0.00393)	968.214(32)	314.36120(14)	296.65566(14)
Carbon-9	1.41925(0.01337)	-1.92689(0.00992)	0	966.70(14)	314.52606(51)	296.12844(42)
Carbon-10	3.86297(0.00168)	-0.4131(0.01587)	0	972.988(47)	311.99443(22)	294.51295(22)
Carbon-11	2.83862(0.00244)	1.44907(0.00477)	-1.08262(0.00659)	967.250(50)	313.09484(23)	295.35581(24)
Carbon-28	-3.75113(0.00152)	0.06198(0.09288)	-0.3247(0.01773)	973.092(41)	312.13755(19)	294.68741(19)
Carbon-29	-4.12659(0.00089)	0.90007(0.00412)	0.91916(0.00409)	970.251(25)	311.42616(11)	294.03976(12)
Carbon-32	-3.03992(0.00142)	-1.15615(0.00376)	0.10123(0.04338)	970.800(30)	313.08667(14)	295.28902(14)
Carbon-33	-2.45152(0.00203)	-2.16476(0.00232)	0.41848(0.01255)	964.326(35)	313.68055(17)	295.26712(17)

[a] The number in parentheses is the Costain error for the coordinate.[12]

[b] The resulting coordinate by Kraitchman analysis was an imaginary number, and has been reported as a value of 0.

[c] The sign of the coordinates is taken from the theoretical atom locations.

IV. Conclusions

The rotational spectra of (*R*)-3-butyn-2-ol (*R*)-camphor and (*S*)-3-butyn-2-ol (*R*)-camphor have been reported. The isotopologues in natural abundance were identified in the spectra allowing for a full carbon substitution structure to be determined. The rotational constants have been compared to theoretical methods that function well for complexes. The experimental constants are all within 1.65% of the theoretical rotational constants. In all cases the second closest theoretical structure to an experimental set of rotational constants was a worse match. A large enough difference in frequency is found to conclude that the lowest energy theoretical formations are the experimentally observed structures. The determination of the complex geometry by Kraitchman analysis was used to confirm the structure after the comparison to the theoretical rotational constants. This confirmation shows that the Kraitchman analysis is not necessary to accurately determine absolute configuration for the chiral tag analysis of camphor, which reduces the time and sample consumption necessary for analysis. This is important as a

Kraitchman analysis measurement requires more time to get good signal to noise ratios on these transitions as the isotopologues are about 1% in natural abundance. This close agreement to theory along with the substitution structures results in the conclusion that the chiral tagging method is able to determine the absolute configuration for camphor and that the theory accurately predicts what is found experimentally. In addition, this technique can function as a complimentary technique to existing techniques and can also mitigate challenging cases where electric dipole components are weak via the induction of the chiral tag.

References

1. Kisiel, Z.; Desyatnyk, O.; Białkowska-Jaworska, E.; Pszczółkowski, L., The structure and electric dipole moment of camphor determined by rotational spectroscopy. *Physical Chemistry Chemical Physics* **2003,** *5* (5), 820-826.
2. Gaussian 09, R. E., M. J. Frisch, G. W. Trucks, H. B. Schlegel, G. E. Scuseria, M. A. Robb, J. R. Cheeseman, G. Scalmani, V. Barone, G. A. Petersson, H. Nakatsuji, X. Li, M. Caricato, A. Marenich, J. Bloino, B. G. Janesko, R. Gomperts, B. Mennucci, H. P. Hratchian, J. V. Ortiz, A. F. Izmaylov, J. L. Sonnenberg, D. Williams-Young, F. Ding, F. Lipparini, F. Egidi, J. Goings, B. Peng, A. Petrone, T. Henderson, D. Ranasinghe, V. G. Zakrzewski, J. Gao, N. Rega, G. Zheng, W. Liang, M. Hada, M. Ehara, K. Toyota, R. Fukuda, J. Hasegawa, M. Ishida, T. Nakajima, Y. Honda, O. Kitao, H. Nakai, T. Vreven, K. Throssell, J. A. Montgomery, Jr., J. E. Peralta, F. Ogliaro, M. Bearpark, J. J. Heyd, E. Brothers, K. N. Kudin, V. N. Staroverov, T. Keith, R. Kobayashi, J. Normand, K. Raghavachari, A. Rendell, J. C. Burant, S. S. Iyengar, J. Tomasi, M. Cossi, J. M. Millam, M. Klene, C. Adamo, R. Cammi, J. W. Ochterski, R. L. Martin, K. Morokuma, O. Farkas, J. B. Foresman, and D. J. Fox, Gaussian, Inc., Wallingford CT, 2016.
3. Stephens, P. J.; Devlin, F. J.; Chabalowski, C. F.; Frisch, M. J., Ab Initio Calculation of Vibrational Absorption and Circular Dichroism Spectra Using Density Functional Force Fields. *The Journal of Physical Chemistry* **1994,** *98* (45), 11623-11627.
4. Grimme, S.; Ehrlich, S.; Goerigk, L., Effect of the damping function in dispersion corrected density functional theory. *Journal of Computational Chemistry* **2011,** *32* (7), 1456-1465.
5. Grimme, S.; Steinmetz, M., Effects of London dispersion correction in density functional theory on the structures of organic molecules in the gas phase. *Phys Chem Chem Phys* **2013,** *15* (38), 16031-42.
6. Weigend, F.; Ahlrichs, R., Balanced basis sets of split valence, triple zeta valence and quadruple zeta valence quality for H to Rn: Design and assessment of accuracy. *Physical Chemistry Chemical Physics* **2005,** *7* (18), 3297-3305.
7. Marshall, F. E.; Sedo, G.; West, C.; Pate, B. H.; Allpress, S. M.; Evans, C. J.; Godfrey, P. D.; McNaughton, D.; Grubbs, G. S., The rotational spectrum and complete heavy atom structure of the chiral molecule verbenone. *Journal of Molecular Spectroscopy* **2017,** *342*, 109-115.
8. Puzzarini, C., Rotational spectroscopy meets theory. *Physical Chemistry Chemical Physics* **2013,** *15* (18), 6595-6607.
9. Suenram, R. D.; Golubiatnikov, G. Y.; Leonov, I. I.; Hougen, J. T.; Ortigoso, J.; Kleiner, I.; Fraser, G. T., Reinvestigation of the Microwave Spectrum of Acetamide. *Journal of Molecular Spectroscopy* **2001,** *208* (2), 188-193.
10. Brown, G. G.; Dian, B. C.; Douglass, K. O.; Geyer, S. M.; Shipman, S. T.; Pate, B. H., A broadband Fourier transform microwave spectrometer based on chirped pulse excitation. *Rev. Sci. Instrum.* **2008,** *79* (5), 053103/1-053103/13.
11. Kisiel, Z. PROSPE - Programs for ROtational SPEctroscopy. http://info.ifpan.edu.pl/~kisiel/prospe.htm.
12. Costain, C. C., Further comments on the accuracy of r-s substitution structures. In *Transactions of the American Crystallograpic Association*, 1966.

Chapter 4

Absolute Configuration Determination of Cedrol

I. Introduction

To further test the ability of chiral tagging to differentiate between enantiomers, the compound (1*S*,2*R*,5*S*,7*R*,8*R*)-2,6,6,8-tetramethyltricyclo[5.3.1.01.5] undecan-8-ol (referred to as (+)-cedrol), shown in Figure 4.1, was chosen. Cedrol was chosen as it is a larger molecule case than camphor (152.237 g/mol) with a molecular weight of 222.37 g/mol. Cedrol also has more chiral centers than camphor potentially creating issues with a higher number of stereoisomers and more complex spectral intensity. The large size could lead to issues differentiating between the tagged species due to a smaller change in rotational constants from the small addition of mass from the tagging molecule. If the difference in rotational constants becomes smaller than the error associated with the measurement, it prevents confident absolute configuration assignment.

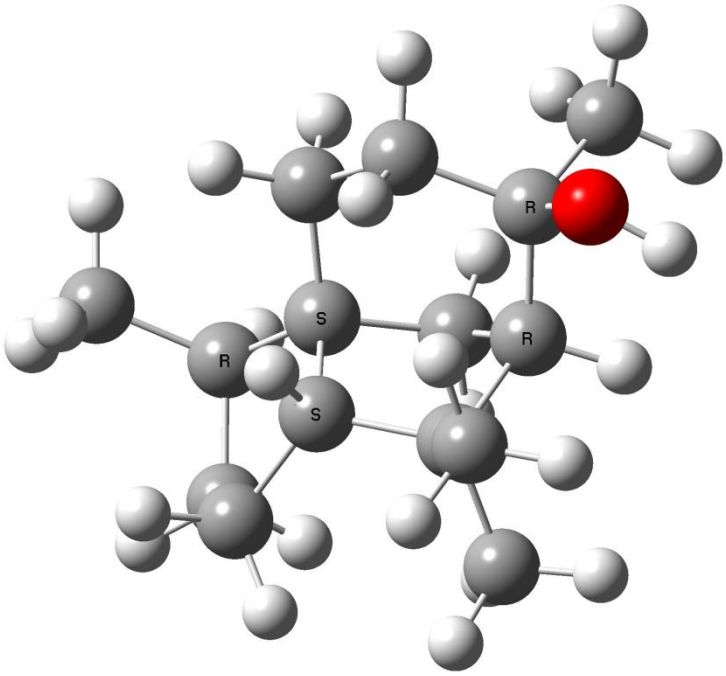

Figure 4.1: The structure of (+)-cedrol shown with stereocenter labels

II. Experimental

Similar to camphor, a tagging molecule had to be chosen to complex with cedrol. In this case, propylene oxide was chosen as it is a small rigid molecule, 58.08 g/mol, and acts as a hydrogen bond acceptor. (+)-Cedrol (≥99.0%) was purchased from Sigma Aldrich® while (*S*)-(-)-propylene oxide (>98%), (*R*)-(+)-propylene oxide (>98.0%) and racemic propylene oxide (>99.0%) were purchased from Tokyo Chemical Industry CO. In this case, a 0.1% propylene oxide in neon gas cylinder was used as the chiral tag, with the neon acting as the carrier gas. Cedrol was heated to approximately 130°C inside of the baseplate within the vacuum chamber and then expanded into vacuum via a supersonic jet expansion.[1] The neon with propylene oxide was used at a pressure of ~16 psig. For the cedrol with enantiopure (*R*)-(+)-propylene oxide, 3,500,000 FID averages were collected, enantiopure (*S*)-(-)-propylene oxide had 1,000,000 FID averages, while racemic propylene oxide had 200,000 FID averages. A (+)-cedrol monomer spectrum was also collected consisting of 375,000 averages. JB95 was once again used to assign

peaks in the experimental spectrum in relation to theoretical rotational constants and these initial fits were further refined through SPFIT and AABS package.[2-3]

Similar to camphor, the complexes formed by cedrol and propylene oxide were calculated by Gaussian 09 Revision E.01 using the B3LYP D3BJ method and the def2-tzvp basis set.[4] Further complicating the quantum calculations, cedrol has an internal rotation of the hydroxyl group and a ring pucker, making it a semi-conformationally flexible molecule. Due to a possible ring pucker, the amount of potential conformations was doubled for the hydroxyl group positions. The possibility of many energetically low-lying conformations necessitates a thorough scan of the potential energy surface. The lowest energy conformation is shown in Figure 4.2 with the structural parameters in Table 4.1. The strongest transitions in the experimental spectra were expected to be the b-type transitions due to the 1.49 Debye dipole moment component along the b principal axis. However, an a-type spectrum of similar intensity was expected due to the similar μ_a and μ_b dipole components.

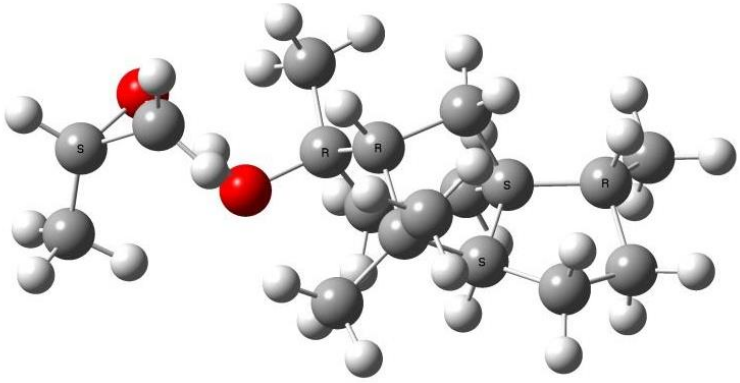

Figure. 4.2: The lowest energy structure found by theoretical calculations

Table 4.1: The structural values of the lowest energy complex for cedrol and propylene oxide

Parameter	Value
A/MHz	684.69
B/MHz	201.24
C/MHz	180.15
μ_a/D	-1.44
μ_b/D	-1.49
μ_c/D	0.90
E/Hartree	-856.0264259

III. Experimental Spectra and Analysis

The experimental spectra for the racemic propylene oxide complexed with (+)-cedrol is shown in Figure 4.3. Within this spectrum there is the potential for (+)-cedrol to form complexes

with both enantiomers of propylene oxide, decreasing enantiopure tag/ analyte complex signal levels. Also included in Figure 4.3 is a plot of the (*R*)-propylene oxide (+)-cedrol experimental spectrum compared to the fitted lowest energy structure of (*R*)-propylene and the fitted lowest energy structure of (*S*)-propylene oxide complexed with (+)-cedrol. This shows the difference in the hetero- and homochiral structures.

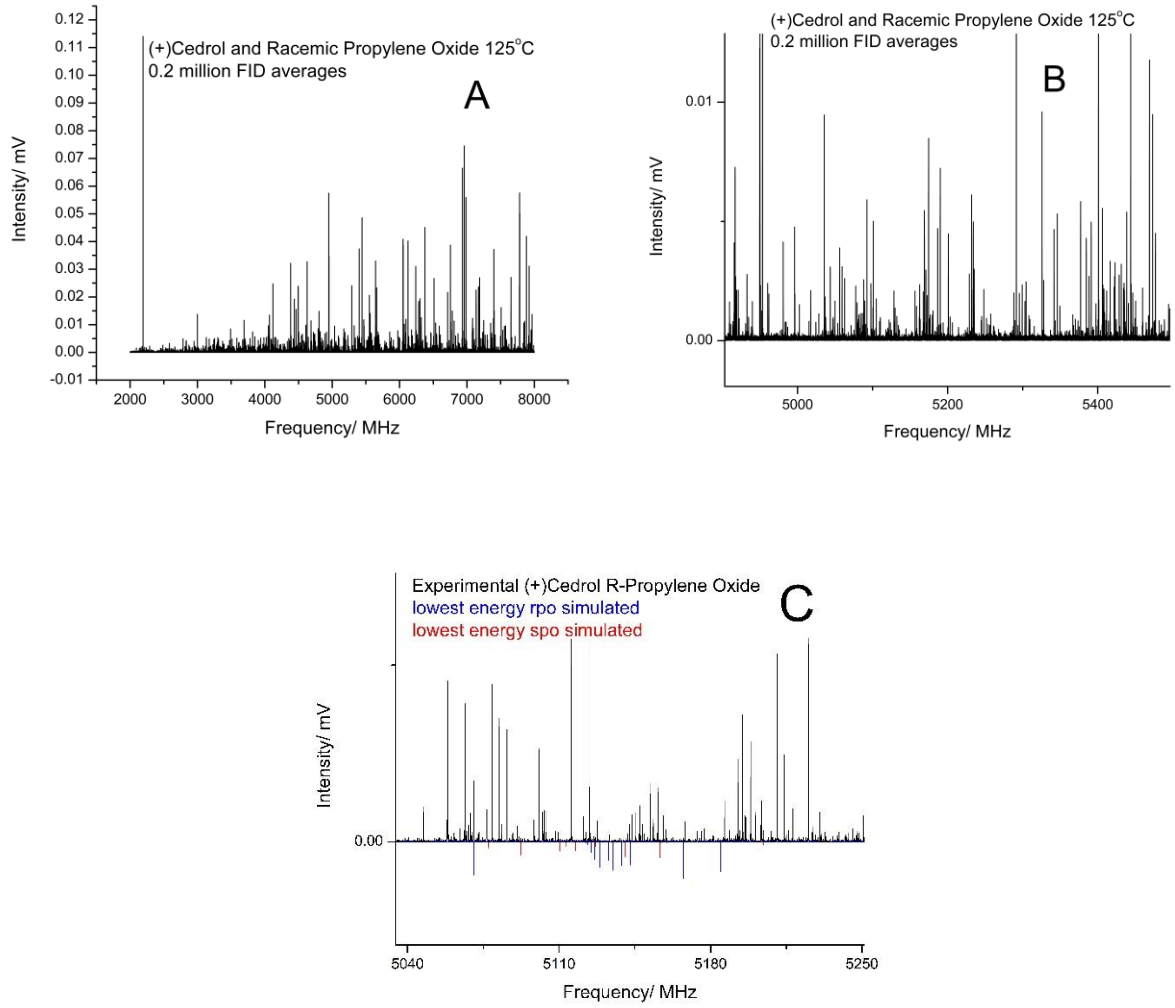

Figure 4.3: The experimental spectra of the different conditions. A shows the racemic propylene oxide complexed with (+)-cedrol, B is a zoomed in section of A showing the complexity of the spectrum. C is R-propylene oxide complexed with (+)-cedrol with the cedrol monomer spectrum cut out compared to the fitted lowest energy theoretical structures of R-propylene oxide and S-propylene oxide complexed with (+)-cedrol.

These spectra are more difficult (compared to camphor) to get a visual idea which tag analyte complex was present due to a more dense spectrum. To determine which complex is present requires the use of a rotational constant comparison; the same comparison was performed with the camphor results. The rotational constants for both stereoisomers of propylene oxide complexed with cedrol have been compared to the experimental rotational constants of the most abundant (*R*)-propylene oxide cedrol complex, shown in Table 4.2. The second theoretical lowest energy levels alongside the lowest theoretical energy levels are compared in Table 4.3.

Table 4.2: The most abundant R-propylene oxide cedrol (R-PO) complex compared to the lowest theoretical energy structures of both enantiomers of propylene oxide complexed with cedrol.

Most abundant R-PO cedrol complex rotational constants			
Rotational Constant	**Experimental (MHz)**	**R-PO lowest energy conformation (MHz)**	**S-PO lowest energy conformation (MHz)**
A	699.49772(25)	698.1 (0.20%)	684.69(2.12%)
B	190.434636(49)	193.6 (1.65%)	201.24 (5.67%)
B	169.594678(56)	172.0 (1.39%)	180.15 (6.22%)

Table 4.3: The two lowest energy theoretical complexes compared to their respective experimental species rotational constants.

Most abundant R-PO cedrol complex			
Rotational Constant	**Experimental (MHz)**	**R-PO lowest energy conformation (MHz)**	**R-PO second lowest energy conformation (MHz)**
A	699.49772(25)	698.1 (0.20%)	700.4 (0.128%)
B	190.434636(49)	193.6 (1.65%)	196.1 (2.99%)
C	169.594678(56)	172.0 (1.39%)	176.7 (4.018%)
Most abundant S-PO cedrol complex			
Rotational Constant	**Experimental (MHz)**	**S-PO lowest energy conformation (MHz)**	**S-PO second lowest energy conformation (MHz)**
A	683.29630(18)	684.69 (0.20%)	708.7 (3.58%)
B	198.798881(67)	201.24 (1.21%)	193.5 (2.74%)
C	178.354363(59)	180.15 (0.97%)	169.8 (5.06%)

The experimental (*R*)-propylene oxide complex has better agreement with the lowest energy theoretical (*R*)-propylene oxide cedrol complex over the (*S*)-propylene oxide cedrol complex, with an average percent error of 1.08 compared to 4.67. When looking at the different theoretical constants compared to the correct tag analyte combination, there is once again much better agreement with the lowest energy complex for the most abundant experimental spectrum. To answer whether cedrol is approaching the limit of this technique for accurately identifying

absolute configuration, a comparison must be done with the rotational constants of the lowest energy complexes seen in Table 4.2 against the percent error of the agreement to the experimental constants. This can be done by taking an average percent error for the theoretical species rotational constants and comparing it to the difference in the theoretical species rotational constants. The uncertainty of both structures has to be added together and compared to the difference to obtain the total accuracy of absolute configuration determination. The difference in the A rotational constant for the experimental lowest energy (*R*)-propylene oxide and (*S*)-propylene oxide (+)-cedrol complexes is 16.20142 MHz. The percent error is 0.200% for the (*R*)-propylene oxide (+)-cedrol complex results in an uncertainty of 1.4 MHz. The percent error for the (*S*)-propylene oxide (+)-cedrol complex results in an uncertainty of 1.4 MHz. This is a total uncertainty of 2.8 MHz, much less than the 16.2 MHz difference. For the B rotational constant, the theoretical difference is 8.364245 MHz, while the experimental percent errors result in a total uncertainty of 5.6 MHz. And the C rotational constant has a difference of 8.759685 MHz, with an uncertainty of 4.2 MHz. This is approaching the difference between the two enantiomeric propylene oxides complexed with (+)-cedrol with the B constant uncertainty being less than 3 MHz off of the difference.

To verify the absolute configuration determination, the substitution structure was obtained for the most abundant (*R*)-propylene oxide (+)-cedrol complex. The singly-substituted ^{13}C isotopologues were detected in natural abundance within the 3.54 million FID average data set. The substitution structure is seen in Figure 4.4 with the coordinates of the structure and rotational constants in Table 4.4. The substitution structure shows good agreement with the lowest energy theoretical structure, with a high Costain value of 0.05969 Å.

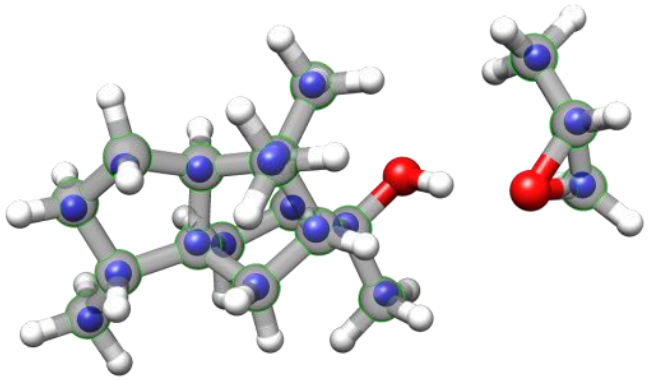

Figure 4.4: The substitution structure of the most abundant (*R*)-propylene oxide (+)-cedrol complex. The blue dots represent the locations of the atoms obtained by Kraitchman analysis within the grey parent structure.

Table 4: List of principal axis coordinates and rotational constants for Kraitchman analysis of the most abundant R-PO complex

Atom-label number	*a*-coordinate Å	*b*-coordinate Å	*c*-coordinate Å	A/MHz	B/MHz	C/MHz
Carbon-2	2.22242(0.00325)[a]	0.39366(0.01841)	0.00[b]	699.356(27)	190.08150(24)	169.30532(17)
Carbon-3	1.82013(0.00328)	-0.98956[c](0.00605)	-0.44957(0.01335)	698.358(22)	190.18272(18)	169.35076(16)
Carbon-4	0.37609(0.01393)	-1.3217(0.00397)	0.00	697.811(19)	190.42448(19)	169.48730(14)
Carbon-5	0.00	0.00	0.75514(0.01169)	698.963(33)	190.39745(29)	169.59862(30)
Carbon-6	1.30577(0.00401)	0.52442(0.00996)	1.31956(0.00398)	697.553(19)	190.18780(17)	169.48193(15)
Carbon-7	3.74362(0.00167)	0.29377(0.0214)	0.41649(0.01509)	699.248(23)	189.42211(24)	168.79605(18)
Carbon-8	1.84169(0.00313)	1.51311(0.00381)	-0.88795(0.00654)	696.536(21)	190.13531(18)	169.27165(17)
Carbon-9	-0.54604(0.0142)	1.12383(0.0069)	-0.26064(0.02988)	698.212(29)	190.40838(24)	169.50588(18)
Carbon-10	3.0512(0.00307)	-1.87572(0.00503)	0.00	696.193(35)	189.77289(41)	168.86795(17)
Carbon-11	4.21735(0.00147)	-0.92396(0.00677)	-0.27579(0.0227)	698.607(23)	189.16119(14)	168.54063(14)
Carbon-12	0.3818(0.01183)	1.40027(0.00321)	-1.33249(0.00341)	695.900(16)	190.29765(17)	169.47429(13)
Carbon-13	0.44523(0.01186)	-2.38495(0.00221)	1.26298(0.00426)	692.519(19)	190.30799(16)	169.25885(13)
Carbon-14	-0.53699(0.00797)	-1.92359(0.00222)	-0.93463(0.00463)	695.099(15)	190.35198(16)	169.36747(13)
Carbon-15	4.59256(0.00191)	1.55864(0.0057)	0.18708(0.04779)	697.146(33)	188.92909(22)	168.26679(20)
Carbon-16	-0.99776(0.01661)	2.39519(0.00694)	0.52476(0.03225)	693.729(62)	190.34363(78)	169.21219(29)
Carbon-43	-5.08314(0.00122)	-0.49939(0.01259)	0.10523(0.05969)	699.249(23)	188.59779(17)	168.12317(16)
Carbon-44	-5.02126(0.00125)	0.96654(0.00656)	0.28809(0.02204)	698.527(23)	188.63613(21)	188.63613(21)
Carbon-48	-4.68353(0.00091)	-1.14995(0.00374)	-1.10644(0.00391)	697.067(15)	188.78677(18)	168.28063(12)

[a] The number in parentheses is the Costain error for the coordinate.[5]

[b] The resulting coordinate by Kraitchman analysis was an imaginary number, and has been reported as a value of 0.

[c] The sign of the coordinates is taken from the theoretical atom locations.

IV. Conclusions

The structure of ((1*S*,2*R*,5*S*,7*R*,8*R*)-2,6,6,8-tetramethyltricyclo[5.3.1.01.5] undecan-8-ol complexed with (*R*)-propylene oxide and (*S*)-propylene oxide has been reported. Rotational spectroscopy was able to be used for this determination due to the chiral tagging method. The complexing in a pulsed jet expansion of the molecules resulted in multiple conformations.

However, the lowest energy conformations of (*R*)-propylene oxide and cedrol complexes have been presented. Further aiding the investigation was the identification of isotopologues in natural abundance. This allowed for the full ^{13}C substitution structure of the most abundant R-PO cedrol complex to be determined. The rotational constants of the experimental species were compared to the theoretical rotational constants for the normal species. The theoretical constants are within 1.65% for the R-PO cedrol complex. The second closest conformation has error greater than 4%. This difference in error shows the accuracy of the theoretical calculations to determine the structures. The substitution structure was also determined by Kraitchman analysis to further verify the experimental structure. The low error between the theoretical structure and experimental structure, along with the verification by Kraitchman analysis, confirms the viability of chiral tagging to function for cedrol. This method should then work with molecules around the same size and flexibility. However, it is starting to get close to encountering difficulty in absolute configuration determination as the percent errors of the theoretical structures when compared to the experimental species are approaching the difference in the rotational constants between the two opposite propylene oxide cedrol complexes.

References

1. Suenram, R. D.; Golubiatnikov, G. Y.; Leonov, I. I.; Hougen, J. T.; Ortigoso, J.; Kleiner, I.; Fraser, G. T., Reinvestigation of the Microwave Spectrum of Acetamide. *Journal of Molecular Spectroscopy* **2001,** *208* (2), 188-193.
2. Pickett, H. M., The fitting and prediction of vibration-rotation spectra with spin interactions. *Journal of molecular spectroscopy* **1991,** *148* (2), 371-377.
3. Z.Kisiel, L. P., I.R.Medvedev, M.Winnewisser, F.C.De Lucia, E.Herbst, J.Mol.Spectrosc. 233,231-243(2005).
4. Gaussian 09, R. E., M. J. Frisch, G. W. Trucks, H. B. Schlegel, G. E. Scuseria, M. A. Robb, J. R. Cheeseman, G. Scalmani, V. Barone, G. A. Petersson, H. Nakatsuji, X. Li, M. Caricato, A. Marenich, J. Bloino, B. G. Janesko, R. Gomperts, B. Mennucci, H. P. Hratchian, J. V. Ortiz, A. F. Izmaylov, J. L. Sonnenberg, D. Williams-Young, F. Ding, F. Lipparini, F. Egidi, J. Goings, B. Peng, A. Petrone, T. Henderson, D. Ranasinghe, V. G. Zakrzewski, J. Gao, N. Rega, G. Zheng, W. Liang, M. Hada, M. Ehara, K. Toyota, R. Fukuda, J. Hasegawa, M. Ishida, T. Nakajima, Y. Honda, O. Kitao, H. Nakai, T. Vreven, K. Throssell, J. A. Montgomery, Jr., J. E. Peralta, F. Ogliaro, M. Bearpark, J. J. Heyd, E. Brothers, K. N. Kudin, V. N. Staroverov, T. Keith, R. Kobayashi, J. Normand, K. Raghavachari, A. Rendell, J. C. Burant, S. S. Iyengar, J. Tomasi, M. Cossi, J. M. Millam, M. Klene, C. Adamo, R. Cammi, J. W. Ochterski, R. L. Martin, K. Morokuma, O. Farkas, J. B. Foresman, and D. J. Fox, Gaussian, Inc., Wallingford CT, 2016.
5. Costain, C. C., Further comments on the accuracy of r-s substitution structures. In *Transactions of the American Crystallograpic Association*, 1966.

Chapter 5

Conclusions

I. Summary

This thesis presents the use of chiral tagging rotational spectroscopy for absolute configuration determination. The technique is tested on two molecules as test cases for viability. The first case tested the accuracy of the chiral tag on a relatively small chiral molecule with one effective chiral center. This test case supported that a direct comparison of the molecule's rotational constants to those of theory accurately identified the absolute configuration of the sample. This result was verified by isotopologue analysis providing the location of the ^{13}C atoms. The use of chiral tagging was extended to a larger molecule to test the ability of the method to confidently determine the absolute configuration of a larger molecules that possess conformational flexibility. The small size of the chiral tag relative to the large analyte can result in diastereomer clusters with similar rotational constants, which affects the confidence of the absolute configuration determination. The same methods of rotational constant comparison and isotopologue analysis verified the absolute configuration identification. However, the difference in rotational constants between the different enantiomers of the chiral tag combined to the molecule approaches the accuracy of the fitted constants. The current theoretical methods are accurate enough to predict the rotational constants of the complexes for absolute configuration determination; however, as larger molecules are tested there will need to be alternate methods to improve the accuracy of the technique. The exceptions being molecules 222.37 g/mol or less, the technique should be able to differentiate between the forms.

II. Future Work

To further establish the abilities of this technique, additional methods need to be explored to ensure the accuracy of the absolute configuration determination. The size difference of cedrol relative to propylene oxide in conjunction with the presence of several low energy conformations challenges the current limit of the technique to accurately determine AC without 13C substitution. The limits of the technique can be extended through development of new chiral tags. The extent of the chiral tagging methods in a mixture also needs to be characterized due to the potential to form complexes with all of the compounds in the sample. This could increase the spectral complexity making it difficult to identify all the species in the spectrum. This is important in pharmaceutical reaction mixtures that have solvent, starting materials, and potential byproducts of synthesis. More conformationally flexible molecules also need to be investigated. An increased number of complexes forming could result in low signal levels preventing accurate absolute configuration determination without longer measurements, as well as increasing spectral complexity. The technique can also be used in collaboration with other techniques for absolute configuration determination. This is relevant to the three-wave mixing technique discussed earlier: to determine the ability of three-wave mixing to accurately identify absolute configuration and enantiomeric excess. The chiral tagging method can be used to obtain a calibration curve for a molecule and then the three-wave mixing technique is used on the same set of samples. This will determine if the three-wave mixing technique can accurately determine enantiomeric excess. Three-wave mixing has the benefit over chiral tagging by not adding additional spectra to be analyzed or needing computationally expensive complex formation theory techniques. Instead, it uses specific frequencies to target individual compounds. This

could augment chiral tagging where the spectral density is too complex for accurate determination.